Dalton Transactions

The strong correlations between thermal conductivities and electronic spin states in crystals of Fe(III) spin crossover complexes

Journal:	*Dalton Transactions*
Manuscript ID	DT-ART-05-2022-001597.R1
Article Type:	Paper
Date Submitted by the Author:	12-Jul-2022
Complete List of Authors:	Hoshino, Norihisa; Niigata University, Department of Materials Science and Technology, Faculty of Engineering Hayashi, Akari; Tohoku University, Graduate School of Engineering Akutagawa, Tomoyuki; Tohoku University, Institute of Multidisciplinary Research for Advanced Materials

ARTICLE

The strong correlations between thermal conductivities and electronic spin states in crystals of Fe(III) spin crossover complexes

Received 00th January 20xx,
Accepted 00th January 20xx

DOI: 10.1039/x0xx00000x

Norihisa Hoshino,*[a] Akari Hayashi,[b] and Tomoyuki Akutagawa[b,c]

Solids that change their thermal conductivity during a phase transition can be useful in the development of a thermal switch to allow control of heat flow and reduce energy consumption. Although a crystal of a spin crossover (SCO) complex is a representative solid with spin states correlated with the heat transporting lattice vibrations, the heat transporting property of a crystal of the SCO complex during a spin state transition has not yet been reported. In this work, we report that the temperature dependence of the thermal conductivity of mononuclear Fe(III) SCO complexes is greatly affected by the spin state transitions. It was determined that the thermal conductivity was minimized at temperatures near the beginning edge of the spin state transitions, and the product of the velocity and the mean free path of the phonon also reached a minimum close to the temperature at which the spin state transition had progressed by 50 %. These findings suggest that the spin state transitions accompanying the coordination bond length elongations and lowering of the vibration energy are allowed at the temperature where the mean-free path of phonons is minimized to the extent of intermolecular distances. These findings also indicate that SCO complexes reported in the literature are promising candidates for heat transportation switch materials.

Introduction

The thermal devices which can control heat flow are likely to be electric devices, such as a switch, a diode, and a transistor, which have received considerable attention for optimizing and reducing thermal energy consumption.[1,2] Although metals and alloys exhibiting metal-insulator transitions during heating/cooling show remarkable on-off ratio at the transition temperatures,[3] the materials with transitions induced by various stimulations such as temperature, light, pressure, and the like. are preferable for more flexible heat flow control. Molecule-based crystals displaying phase transitions induced by various stimulations have been extensively studied;[4] however, thermal conductivity measurements during the phase transitions of such crystals have rarely been reported. In general, molecule-based crystals are fragile and cannot sufficiently grow centimeter-sized crystals to enable the measurement of thermal conductivity using commercial thermal conductivity meters. Recently, in the research field of molecule-based conductors, there have been numerous efforts to overcome such problems,[5–11] which have allowed the evaluation of thermal conductivity properties of small and fragile molecular crystals exhibiting phase transitions.[12,13]

Crystals of spin crossover (SCO) complexes are representative solids with phase transitions induced by various stimuli, such as temperature, light (LIESST), pressure, and guest molecules.[14–16] The transition behaviors of SCO complexes are largely affected by small differences, such as counter ions, substituent groups, and crystal solvents. The heat capacity measurement of $[Fe(NCS)_2(phen)_2]$ during SCO transitions revealed that the spin entropy is much smaller than the overall transition entropy.[17,18] The remaining entropy was considered to be the phonon entropy resulting from the elongation of the coordination lengths accompanied by a lowering of the vibration frequencies; hence, the electronic state of the SCO transitions is strongly correlated with the phonons. As heat is transported by phonons, thermal conductivity measurements can be a useful tool for inspecting the crystal state during spin–state transitions. However, to the best of our knowledge, the thermal conductivity of an SCO complex during spin state transition has not yet been reported.

Crystals of the family of $[Fe(R\text{-}salEen)_2]X$ complexes are one of the most representative series of SCO behaviors studied in detail, except for thermal conductivity.[19–34] In this work, the four derivatives having solvent-free crystals with the potential to be grown to a sufficiently large size for the measurement of thermal conductivity were selected. Herein, the crystal structures, magnetic properties, thermal conductivities, and

[a] Department of Materials Science and Technology, Faculty of Engineering, Niigata University. 8050 Ikarashi-2, Niigata 950-2181, Japan. E-mail: hoshino@eng.niigata-u.ac.jp
[b] Graduate School of Engineering, Tohoku University. 6-6 Aza-aoba, Aramaki, Aoba-ku, Sendai 980-8579, Japan.
[c] Institute of Multidisciplinary Research for Advanced Materials (IMRAM), Tohoku University. 2-1-1 Katahira, Aoba-ku, Sendai 980-8577, Japan.

† Electronic Supplementary Information (ESI) available: Sample preparation methods, crystallographic parameters, coordination bond lengths, numbering schemes for the crystal structure, thermal ellipsoid views, electron-density maps, temperature-dependent unit-cell constants, crystal packing structures, and heat capacity data. CCDC 2160265-2160272, 2184630-2184636. See DOI: 10.1039/x0xx00000x

estimates of the phonon velocity and mean free path of phonons of the four Fe(III) SCO complexes $[Fe(R\text{-}salEen)_2]X_2$ (Fig. 1, **1** : R = H, $X^- = NO_3^-$; **2** : R = H, $X^- = OTf^-$; **3** : R = 5-Br, $X^- = OTf^-$; **4** : R = 3,5-Cl_2, $X^- = OTf^-$, $OTf^- = CF_3SO_3^-$) are reported. The relationship between the spin-state transitions, thermal conductivities, and phonon states of the crystals is further discussed.

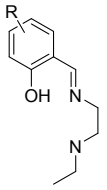

H(R-salEen)

Fig. 1 A structure of H(R-salEen) ligand.

Results and Discussion

Experimentals

H(R-salEen) ligands were prepared by condensation of the corresponding salicylaldehydes and N-ethylethylenediamine in MeOH.[19] Large solvent-free crystals of **1–4** were obtained by the reaction between H(R-salEen), Et_3N, and $Fe(NO_3)_3{\cdot}6H_2O$ or $Fe(OTf)_3{\cdot}6H_2O$. Detailed methods are described in the Supporting Information. The single-crystal and powder X-ray diffraction data were collected using a Rigaku Rapid-II diffractometer (Rigaku). Magnetic properties were measured using an MPMS-5S magnetometer (Quantum Design). Thermal conductivity measurements were performed using a comparative steady-state method using a homemade apparatus described in the literature.[12,13]

Crystal structures

Although the physical properties of crystal **1** have been studied in detail,[19] the crystal structure of **1** has not yet been reported. A thermal ellipsoid plot for the $[Fe(salEen)]^+$ cations in crystal **1** at 100 K is shown in Fig. 2. The three coordination atoms, O(phenoxy), N(imino), and N(amino), in the $salEen^-$ ligand are communicating with the central Fe^{3+} ion with meridional geometry. Six coordination atoms in the two $salEen^-$ ligands occupy all of the coordination sites of Fe^{3+} in the octahedral environment. The $[Fe(R\text{-}salEen)]^+$ cations in crystals **2–4** have the same structural arrangement, as shown in Fig. 2.

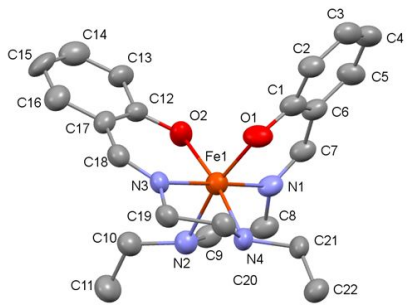

Fig. 2 A thermal ellipsoid view of a cation in crystal **1** at 100 K.

The selected coordination bond lengths at 100 K, 300 K, T_κ, and T_{vl} (Table 1) are shown in Table S2, along with the numbering schemes in Fig. S1. Two independent cations, Fe1 and Fe2, were included in crystals **1** and **2**, whereas only one independent cation, Fe1, was included in crystals **3** and **4**. At 100 K, the coordination bond lengths of **2–4** are in the typical range of the LS Fe(III) complex, which is in good agreement with the $\chi_m T$ values in Fig. 3 (see the magnetic property section). In crystal **1**, the coordination bonds to Fe2 have almost the same length as those in **2–4**, whereas the bonds around Fe1 are slightly longer than those of Fe2. As the $\chi_m T$ value of crystal **1** (1.55 $cm^3\ mol^{-1}\ K$) at 100 K is close to the spin-only value for the mixture of HS:LS = 7:3 (4.375×0.7 + 0.375×0.3 = 1.575), the site at Fe1 is probably disordered for the HS and LS complex while the Fe2 site is completely occupied by the LS complex. At 300 K, the coordination environment of Fe^{3+} ions in **1** is much more elongated than that at 100 K, corresponding to spin state transitions, where the bond lengths of Fe1 are typical values of the HS Fe^{3+} ions, whereas the bond lengths of Fe2 at 300 K are intermediate between those of the HS and LS states. Hence, at 300 K, the Fe1 site is completely in the HS state, whereas the Fe2 site is disordered by HS and LS Fe^{3+} ions.

In crystal **1**, the two cations of Fe1 and Fe2 are connected to the two NO_3^- ions (Fig. S2), where the four hydrogen atoms (H1–H4) attached to the four secondary amines (N1–N4) are close to the oxygen atoms of the two NO_3^- ions (O5–O10). Such cation-anion-cation interactions through could cause two-step spin state transitions in crystal **1**. In the transition from the LS to HS state, the coordination bond length of the Fe-N(amino) is elongated, and the vibration energy state is relaxed. Therefore, the thermal displacement of the NO_3^- anion can be correlated with the spin state of the Fe^{3+} ions via the stretching vibration of the coordination bond. The cations in **2**-**4** are not dimerized like those in **1** because of the amphiphilic character of the OTf^- anion, which consists of a hydrophobic $-CF_3$ unit and a hydrophilic $-SO_3$ unit. In crystals **2**-**4**, an $[Fe(R\text{-}salEen)_2]^+$ cation is bound to an OTf^- anion via hydrogen bonding, as shown in Fig. S3. The thermal displacement of OTf^- can also be related to the spin state through Fe–N (amino) bond elongations and vibration frequency lowering.

The temperature-dependent thermal ellipsoid views of the NO_3^- anions in **1** and OTf^- anions in **2–4** are shown in Fig. S4. Increasing the temperature inflates the thermal ellipsoids of NO_3^- in crystal **1** and OTf^- in crystals **2–4**. The elongated shape of NO_3^- in **1** seems to be retained from 100 to 300 K, whereas the O and F atoms of OTf^- in **2–4** are flattened without anisotropic elongation. This suggests that isotropic thermal displacements, rather than rotational vibrations, are increased during heating, which is consistent with the isotropic peaks in the electron-density maps in Fig. S5.

Temperature-dependent unit-cell constants and volumes for **1–4** in the temperature range of 100–300 K are also shown in Fig. S6. The *b*- and *c*-axis lengths of **3** exhibited anomalies around $T_{\kappa 3}$ and T_{vl3}, corresponding to spin transition (see below). However, no other anomalies was found in the unit-cell constants and volumes, suggesting a gradual increase in the thermal displacements during heating.

Crystal packing structures are shown in Fig. S8. Except for the cation-anion hydrogen bonding described above, strong interactions such as hydrogen bonding, halogen-halogen, and π-π interaction were not found among cations in **1–4.** Absence of intermolecular interaction in the SCO crystals implies gradual spin-state transitions without cooperativity. [14,19]

Magnetic properties

Magnetic susceptibilities were measured for granules of crystals **1–4** in the range of 10–300 K at a sweep rate of 2 K/min. No hysteresis was observed between the cooling and heating processes for complexes **1–4**. The $\chi_m T$ versus T plots during heating are shown in Fig. 3. Note that the data for **1** are in good agreement with the literature data.[19] The $\chi_m T$ value of **1** at 10 K was 1.28 cm^3 mol^{-1} K, which is much higher than the spin-only value for the LS Fe^{3+} ion (0.375 cm^3 mol^{-1} K for g = 2.0, s = 1/2). According to the Mössbauer data in the literature, an intermediate spin state is not observed, but a small amount of the HS Fe^{3+} ion was present in crystal **1** at 10 K. Crystal **1** shows a broad two-step spin state transition, where the first step begins at T_{A1} = 74 K and the second step begins at T_{B1} = 220 K. The $\chi_m T$ value of **1** at T_{B1} was 2.46 cm^3 mol^{-1} K, which is close to the spin-only value of the HS:LS = 1:1 mixture (4.375×0.5 + 0.375×0.5 = 2.375). The LS-to-HS transition was not completed below 300 K, which is the limit of thermal conductivity measurements using our apparatus.

Crystals **2–4** also exhibited a gradual spin transition above 200 K; however, the transitions were not completed within the experimental limit of 300 K. The $\chi_m T$ values of **2–4** were 0.43, 0.51, and 0.43 cm^3 mol^{-1} K, respectively, which are close to the spin-only value for the LS Fe^{3+} ion. As the temperature was raised, the $\chi_m T$ of **3** began rising at T_{A2} = 200 K and reached 2.39 cm^3 mol^{-1} K at T_{B2} = 278 K, which is close to the spin-only value for the mixture of HS:LS = 1:1. In crystal **2**, only the beginning of the transition could be observed at T_{A3} = 240 K, whereas the transition of **4** was hardly observed within the limit of the measurement range below 300 K.

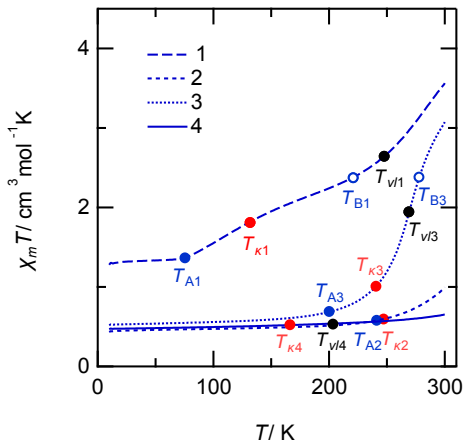

Fig. 3 $\chi_m T$ vs. T plots for crystals **1–4** in the range of 10-300 K during heating at a sweep rate of 2 K/min. The blue filled circles indicate the rising edge of $\chi_m T$, and the blue open circles indicate the points at which $\chi_m T$ is the spin-only value for HS:LS = 1:1 (2.375 cm^3 mol^{-1} K). The red and black points indicate the temperatures at which the κ or vl values are minimized, as shown in Fig. 4 and 5.

Thermal conductivities

Thermal conductivity measurements were performed during the cooling of crystals **1–4**. The measurements were started at 300 K because of the limitation of the apparatus, and the lowest temperatures were also limited by the cracking of the crystal along the cleavage plane. The temperature-dependent thermal conductivities of **1–4** are shown in Fig. 4 along with a summary of the related parameters in Table 1.

At 300 K, crystal **1** exhibited the highest thermal conductivity of **1**–**4**, corresponding to its lowest molecular weight. The κ values at 300 K followed the order of molecular weight and crystal density. In general, the velocity of phonons that transport heat in a solid decreases as the molecular mass increases. As the temperature decreased, the κ values decreased and reached the minimum value κ_{min} at the indicated temperature $T_{\kappa 1}$ – $T_{\kappa 4}$ (Fig. 4). Below the minimum, the κ values increased as the temperature decreased. In general, a negative temperature coefficient of thermal conductivity is observed in crystalline materials, whereas a positive coefficient is observed in glassy materials. Note that the temperature coefficient transitions between positive and negative have been found in some molecular crystals showing order-disorder transitions.[12,13] In Fig. 3 and 4, the temperatures at which the thermal conductivity is minimized ($T_{\kappa 1}$, $T_{\kappa 2}$, and $T_{\kappa 3}$) are close to the temperature at which the spin-state transitions begin (T_{A1}, T_{A2}, and T_{A3}). This clearly suggests that the thermal conductivity correlates with the spin state of the Fe^{3+} ions in crystals **1–3**. In contrast, crystal **4** displayed the minimum thermal conductivity at $T_{\kappa 4}$ = 166 K, despite a lack of spin-state transition below 300 K.

Table 1 Parameters for the thermal conductivities and magnetic susceptibility data for **1–4**.

Crystal	1	2	3	4
κ at 300 K [a]	0.281	0.177	0.118	0.163
density at 300 K	1.390	1.486	1.710	1.541
formula weight	500.36	587.42	745.22	725.19
κ_{min} at T_κ [a]	0.192	0.168	0.098	0.101
T_κ / K	128	248	232	166
T_A / K	74	240	200	-
T_{vl} / K	246	> 300	254	206
T_B / K	220	> 300	277	-

[a] Unit for thermal conductivity: W m^{-1} K^{-1}.

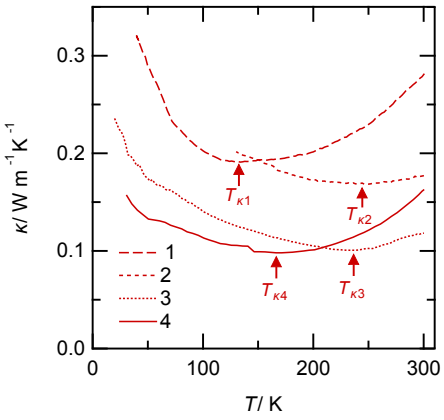

Fig. 4 Thermal conductivities of crystals **1**–**4**.

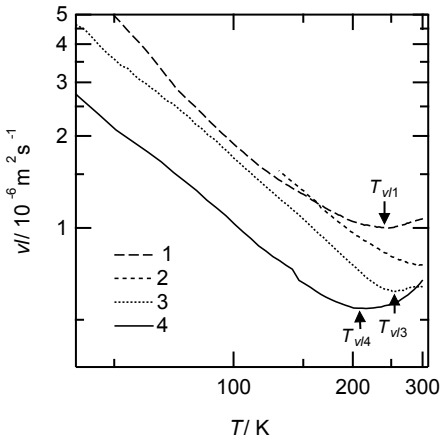

Fig. 5 *vl* vs *T* plots for crystals **1**–**4** calculated by $\kappa = 1/3Cvl$.

Mean free path of phonons and spin state transitions

In simple kinetics, the thermal conductivity κ is expressed as $\kappa = 1/3Cvl$, where C is the specific heat; v is the phonon velocity; and l is the free mean path of a phonon. In this work, the heat capacities of **1**–**4** were measured by the relaxation method, and their specific heats were estimated, as shown in Fig. S7. v has not been determined experimentally; however, it depends on the elastic stiffness of the crystal, which is expected to show a lesser temperature dependence than C.[38] The vl values were calculated using the measured κ ,and the estimated C values were used to study the temperature dependence of the mean free path of the phonons in crystals **1**–**4**.

The vl vs. T plots for **1**–**4** complexes are shown in Fig. 5. As the temperature was increased, the vl values of **1**–**4** decreased following the function of T^{-1}, similar to general crystalline materials. The vl values of **1**, **3**, and **4** reached the minimum value at temperature T_{vl} (Table 1), and the vl of **2** reached approximately 300 K. Above T_{vl1} and T_{vl3}, the vl values of **1** and **3** are almost temperature independent, because the l values are minimized to the intermolecular distances.[2,35] The gradual increase in the vl values above the minima at T_{vl1}, T_{vl3}, and T_{vl4} can be artifacts resulting from the simplistic kinetic model deriving $\kappa = 1/3Cvl$. T_{vl1} and T_{vl3} are indicated in Fig. 3 and are very close to T_{B1} and T_{B3}, respectively. This means that the mean free path of the phonons in **1** and **3** was minimized in the spin-state transition near the temperature where the ratio of HS:LS is 1:1.

Phonon states during spin state transition

As described above, as the temperature was increased, the thermal conductivity κ of **1**–**4** decreased, reaching a minimum, and then increased with further heating. A schematic of the phonon states during heating is shown in Fig. 6. At a low temperature T, where the transportation of phonons is ballistic (Fig. 6a), the mean free path of phonon l depends on the frequency of the phonon-phonon scattering. Because the number of phonons is proportional to T, l and κ are inversely proportional to T.[1,36] At a certain temperature, l is minimized to l_{min}, which is close to the intermolecular distance (Fig. 6b). With further heating, l is constant at l_{min}, where the transportation of phonons is diffusive (Fig. 6c). The number of phonons is still proportional to T, and the lattice heat capacity C and κ increase as T increases.

As shown in Fig. 3 and Table 1, the thermal conductivities and spin state transitions were correlated in crystals **1**–**3**. The temperature at which the thermal conductivity was minimized (T_κ) was close to the initial edge temperature of the spin-state transition (T_A), whereas the temperature at which the vl value was minimized (T_{vl}) was close to the temperature at which the HS:LS ratio was 1:1 (T_B). Such a correlation between the thermal conductivity and spin state could be induced by the vibronic coupling between the coordination bonds and phonons; elongation of the coordination bond lengths, accompanied by a decrease in the vibrational frequencies, could be attributed to the lattice vibrations.[17,18] In addition, hydrogen bonding between the coordinating N (amino) and O atoms in the NO_3^- or the OTf^- anions could affect their thermal displacements (Figs. S2 and S3); fluctuating and disordered anions can scatter the heat-transporting phonons and minimize their mean free path.[2,37] Although the lattice constants do not change abruptly around T_κ and T_{vl}, as shown in Fig. S6, it is noteworthy that the mean free path of the phonons is expected to be a function of T^{-1} and be minimized in general crystalline solids without spin-state transitions nor abrupt structural changes.[36] Hence, the lack of correlation between $T_{\kappa4}$ and the spin-state transition in **4** is justified, because the spin-state transition temperature is much higher than $T_{\kappa4}$. This also suggests that thermal conductivity can be correlated with the spin-state transition

only in the temperature range wherein the phonon transportation is ballistic and their mean free path can be modulated by the spin state. Further experiments on similar SCO materials, such as neutral crystals and glassy solids, could clarify the main contributor to the thermal conductivity.

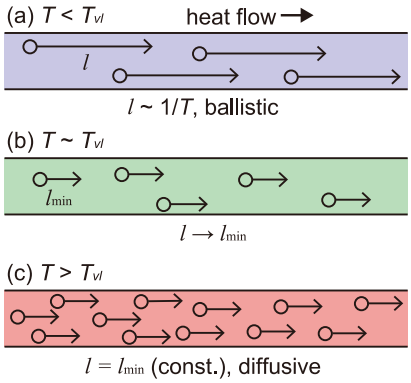

Fig. 6 A schematic drawing of phonons during heating.

Conclusions

The magnetic susceptibilities and thermal conductivities were compared for crystals **1**–**4**. The thermal conductivities were minimized near the rising edge temperature of the $\chi_m T$ values for **1**–**3**. The heat capacities were also measured, and the products of the phonon velocity v and mean free path l of the phonons were estimated using $\kappa = 1/3Cvl$. For **1** and **3**, the vl values reached a minimum close to the temperature at which $\chi_m T$ was the expected value for HS:LS = 1:1. To the best of our knowledge, this is the first report to reveal the relationship between the thermal conductivity and the spin state of a crystal of an SCO complex. In this study, only SCO complexes showing gradual spin state transitions were studied. SCO complexes showing abrupt spin-state transitions with thermal hysteresis, as well as complexes showing light-induced spin-state transitions, can be used in the development of novel solid-state thermal switching materials.

Acknowledgements

This work was financially supported by a Grant-in-Aid for Scientific Research (C; No. 20K05535) from the Ministry of Education, Science and Culture of Japan (MEXT), CREST (No. JPMJCR18I4) by the Japan Science and Technology Agency, the Grant for Basic Science Research Projects (No. 200296) by the Sumitomo Foundation, the Grant for Science Research by the Shorai Foundation for Science and Technology, the Grant for Science Research by the Tokuyama Science Foundation, the Grant for Science Research (0341159-A) by the Iketani Science and Technology Foundation, and the "Dynamic Alliance for Open Innovation Bridging Human, Environment, and Materials" by MEXT.

Conflicts of interest

There are no conflicts to declare.

References

1 T. M. Tritt, Ed., *Thermal conductivity: theory, properties, and applications*, Kluwer Academic/Plenum Publishers, New York, 2004.
2 V. A. Konstantinov, in *Heat Transfer - Theoretical Analysis, Experimental Investigations and Industrial Systems*, ed. A. Belmiloudi, InTech, 2011.
3 S. Lee, K. Hippalgaonkar, F. Yang, J. Hong, C. Ko, J. Suh, K. Liu, K. Wang, J. J. Urban, X. Zhang, C. Dames, S. A. Hartnoll, O. Delaire and J. Wu, *Science*, 2017, **355**, 371–374.
4 M. Irie, Y. Yokoyama and T. Seki, Eds., *Photomechanical Response of Diarylethene Single Crystals*, Springer Japan, Tokyo, 2013.
5 M.-Y. Choi, P. M. Chaikin and R. L. Greene, *Phys. Rev. B*, 1986, **34**, 7727–7732.
6 P. B. Allen, X. Du, L. Mihaly and L. Forro, *Phys. Rev. B*, 1994, **49**, 9073–9079.
7 K. Torizuka and H. Tajima, *Review of Scientific Instruments*, 2005, **76**, 033908.
8 K. Torizuka, H. Tajima and T. Yamamoto, *J. Phys. Soc. Jpn.*, 2006, **75**, 074604.
9 H. Yoshino, G. C. Papavassiliou and K. Murata, *J Therm Anal Calorim*, 2008, **92**, 457–460.
10 H. Yoshino, G. C. Papavassiliou and K. Murata, *Synthetic Metals*, 2009, **159**, 2387–2389.
11 Y. Iwasaki, H. Yoshino, N. Kuroda, K. Kikuchi and K. Murata, *J. Phys. Soc. Jpn.*, 2015, **84**, 054601.
12 N. Hoshino and T. Akutagawa, *J. Chem. Phys.*, 2020, **153**, 194503.
13 N. Hoshino, S. Tamura and T. Akutagawa, *Chem. Eur. J.*, 2020, **26**, 2610–2618.
14 O. Kahn, *Molecular magnetism*, Wiley-VCH, New York (N.Y.), 1993.
15 P. Gütlich and H. A. Goodwin, Eds., *Spin crossover in transition metal compounds I-III*, Springer-Verlag, Berlin, 2004.
16 M. A. Halcrow, Ed., *Spin-crossover materials: properties and applications*, Wiley, Chichester, West Sussex, United Kingdom, 2013.
17 M. Sorai and S. Seki, *J. Phys. Soc. Jpn.*, 1972, **33**, 575–575.
18 M. Sorai and S. Seki, *Journal of Physics and Chemistry of Solids*, 1974, **35**, 555–570.
19 M. S. Haddad, M. W. Lynch, W. D. Federer and D. N. Hendrickson, *Inorg. Chem.*, 1981, **20**, 123–131.
20 M. D. Timken, D. N. Hendrickson and E. Sinn, *Inorg. Chem.*, 1985, **24**, 3947–3955.
21 M. Wang, G.-H. Lee, Y. Wang, T.-Y. Dong and H.-H. Wei, *J. Chin. Chem. Soc.*, 2002, **49**, 825–832.
22 S. Hayami, S. Miyazaki, M. Yamamoto, K. Hiki, N. Motokawa, A. Shuto, K. Inoue, T. Shinmyozu and Y. Maeda, *BCSJ*, 2006, **79**, 442–450.
23 C. Faulmann, K. Jacob, S. Dorbes, S. Lampert, I. Malfant, M.-L. Doublet, L. Valade and J. A. Real, *Inorg. Chem.*, 2007, **46**, 8548–8559.
24 A. Tissot, R. Bertoni, E. Collet, L. Toupet and M.-L. Boillot, *J. Mater. Chem.*, 2011, **21**, 18347–18353.
25 C. Faulmann, J. Chahine, L. Valade, G. Chastanet, J.-F. Létard and D. de Caro, *Eur. J. Inorg. Chem.*, 2013, **2013**, 1058–1067.

26 C.-F. Sheu, S.-M. Chen, G.-H. Lee, Y.-H. Liu, Y.-S. Wen, J.-J. Lee, Y.-C. Chuang and Y. Wang, *Eur. J. Inorg. Chem.*, 2013, **2013**, 894–901.
27 A. Tissot, P. Fertey, R. Guillot, V. Briois and M.-L. Boillot, *Eur. J. Inorg. Chem.*, 2014, **2014**, 101–109.
28 P. N. Martinho, A. I. Vicente, S. Realista, M. S. Saraiva, A. I. Melato, P. Brandão, L. P. Ferreira and M. de D. Carvalho, *Journal of Organometallic Chemistry*, 2014, **760**, 48–54.
29 W. Phonsri, V. Martinez, C. G. Davies, G. N. L. Jameson, B. Moubaraki and K. S. Murray, *Chem. Commun.*, 2016, **52**, 1443–1446.
30 A. I. Vicente, A. Joseph, L. P. Ferreira, M. de D. Carvalho, V. H. N. Rodrigues, M. Duttine, H. P. Diogo, M. E. M. da Piedade, M. J. Calhorda and P. N. Martinho, *Chem. Sci.*, 2016, **7**, 4251–4258.
31 F. F. Martins, A. Joseph, H. P. Diogo, M. E. Minas da Piedade, L. P. Ferreira, M. D. Carvalho, S. Barroso, M. J. Romão, M. J. Calhorda and P. N. Martinho, *Eur. J. Inorg. Chem.*, 2018, **2018**, 2976–2983.
32 A. I. Vicente, L. P. Ferreira, M. de D. Carvalho, V. H. N. Rodrigues, M. M. Dîrtu, Y. Garcia, M. J. Calhorda and P. N. Martinho, *Dalton Trans.*, 2018, **47**, 7013–7019.
33 T. Boonprab, P. Harding, K. S. Murray, W. Phonsri, S. G. Telfer, A. Alkaş, R. Ketkaew, Y. Tantirungrotechai, G. N. L. Jameson and D. J. Harding, *Dalton Trans.*, 2018, **47**, 12449–12458.
34 T. Boonprab, S. J. Lee, S. G. Telfer, K. S. Murray, W. Phonsri, G. Chastanet, E. Collet, E. Trzop, G. N. L. Jameson, P. Harding and D. J. Harding, *Angew. Chem. Int. Ed.*, 2019, **58**, 11811–11815.
35 C. Kittel, *Phys. Rev.*, 1949, **75**, 972–974.
36 C. Kittel, *Introduction to Solid State Physics*, John Wiley & Sons, Inc., New York, Seventh Ed., 1996.
37 W. Bausch, W. Waidelich, *Physics Letters A*, 1969, **30**, 190–191.
38 K. W. Böer and U. W. Pohl, *Semiconductor Physics*, Springer, Cham, 2014.